Neues Jahrbuch Miner. Abh.	146	2	133–150	Stuttgart, April 1983

High-TiO_2 basaltic dikes in the coastline of São Paulo and Rio de Janeiro States (Brazil)

By

P. Comin-Chiaramonti, Trieste, **C. B. Gomes,** São Paulo, **E. M. Piccirillo,** Trieste, and **G. Rivalenti,** Ferrara

With 10 figures and 5 tables in the text

Comin-Chiaramonti, P., Gomes, C. B., Piccirillo, E. M. & Rivalenti, G.: High-TiO_2 Basaltic dikes in the coastline of São Paulo and Rio de Janeiro States (Brazil). – Neues Jahrbuch Miner. Abh. **146:** 133–150; Stuttgart 1983.

Abstract: Mesozoic dike swarms trending NE-SW are widespread in the pre-Cambrian crystalline basement outcropping along the coastline of São Paulo and Rio de Janeiro States (Southern Brazil).

The dikes are represented by latibasalt and andesi-basalt rock types characterized by high TiO_2 (up to 5 %), as well as high P, Zr, Ba, Sr and Rb contents.

Petrographical, geochemical and mineralogical data show that the dikes have a well-defined transitional character with alkaline or, subordinately, tholeiitic affinity.

The comparison between the dikes and the "coeval" high-TiO_2 rock-types of the stratoid basaltic volcanics and sills of the Paranà basin reveal a tholeiitic to transitional compositional variation of the W-E trending Lower Cretaceous Brazilian magmatism.

Key words: Basalt (lati-basalt, andesi-basalt), dolerite, dikes, major elements, Ti, trace-element analyses (Zr, Ba, Sr, Rb), electron probe data, clinopyroxene, pigeonite, titanomagnetite, ilmenite, olivine; Lower Cretaceous, São Paulo, Rio de Janeiro.

Introduction

Dike swarms of basic rocks are widespread along the Serra do Mar (Fig. 1) in Southern Brazil (Damasceno, 1966). This activity occurred during the Lower Cretaceous (124–138 m.y.; Amaral et al., 1966; Minioli et al., 1971; Siedner & Mitchell, 1976) and was then at least partly "coeval" with the stratoid basalt volcanism of the Paranà basin (Serra Geral formation: 120–135 m.y.; Amaral et al., 1966; Melfi, 1967; Minioli et al., 1971 and references therein). This fact is obviously of great interest both from the magmatological and geotectonic viewpoints, since dike activity can really be related to the Serra Geral volcanism (cfr. Minioli et al., 1971 and references therein), and hence allows us to obtain relevant data on the nature of the magmatic activity which occurred towards the easternmost part of the Paranà basin.

The dikes are subvertical to vertical and, as a rule, appear regular, straight and parallel in shape. They vary in size, occasionally reaching many meters in

0077-7757/83/0146-0133 $ 4.50

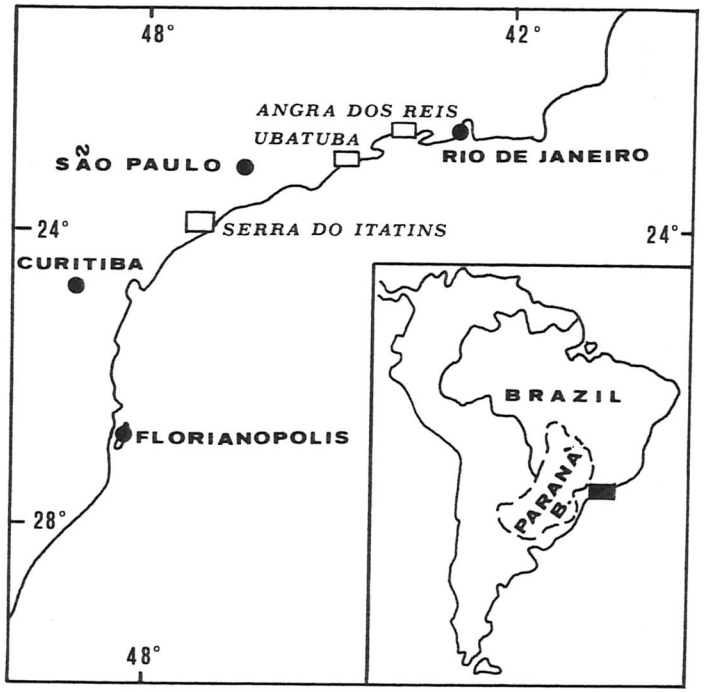

Fig. 1. Sketch map showing location of sampled areas. Numbers represent analysed dikes, following Table 1.

width and a few kilometres in length. The Toninhas dike, outcropping near the city of Ubatuba, represents the most impressive body, having a width of approximately 90 meters. This dike was investigated in some detail (Gomes, 1974; Gomes & Ruberti, 1979; Gomes & Berenholc, 1980), but only a general description is available for all the other numerous dikes (about 90; Damasceno, 1966) occurring along a 70 km coast section in the Caraguatatuba-Ubatuba region.

The dikes studied trend predominantly N 40–50 E (N 25 W and E–W directions are rare) and are parallel to the regional structure lineaments of the host pre-Cambrian crystalline basement (gneiss, migmatitic and charnockitic rocks).

The dikes were sampled from Serra dos Itatin near Peruibe, and along the BR-101 highway, between Ubatuba, San Paulo, and Angra dos Reis, Rio de Janeiro (about 180 km; Fig. 1).

Except for the Serra dos Itatin samples (nos. 4, 10 and 21), all the remaining ones were collected at or near the contact with the country rocks, since these "chilled" margins may reasonably be considered representative of liquid compositions.

Petrographic outlines

The dikes, mainly represented by andesi-basalt and latibasalt (see later), are characterized by three main textures: doleritic, "quench" and porphyritic.

Doleritic dikes (1, 2, 10, 11, 12, 15, 16, 20, 21 of Tables 1 a and 1 b) have fine to coarse grain size. In order of appearance, the most abundant minerals are: opaques (Ti-magnetite and ilmenite), plagioclase (An 65–30) and augite (Wo 45–32). Apatite (up to 0.5 mm) is frequently found, while biotite and amphibole (the latter produced by pyroxene transformation) are scarce and sporadic.

Ca-rich clinopyroxene is frequently pinkish-coloured in the latibasaltic types and rarely (sample 15) in the andesi-basalt rock plotting near the latibasalt boundary (Fig. 2). In two cases (samples 10 and 20) pigeonite microphenocrysts are found associated with pale greenish augite. Olivine phenocrysts occur only in one sample (20) with composition between Fa 73 and Fa 75, coexisting with Ca-rich pyroxene (Wo 35–33).

Andesi-basalt doleritic dikes are commonly characterized by interstitial graphic quartz-alkali feldspar intergrowths. The same type of texture also occurs in sample 20 belonging to the latibasalt group.

"Quench dikes" (5, 7, 8, 9, 13, 14, 17, 18, 19 of Tables 1 a and 1 b) mainly straddle the latibasalt/andesi-basalt boundary (Fig. 2). They usually have pheno- or microphenocrysts of Ti–magnetite, plagioclase (An 60–45) and augite (Wo 35). Only very elongated ilmenite and/or Ca-rich clinopyroxene crystals may be recognized in the groundmass. Large xenocrysts (up to 1 cm) of plagioclase (An 45–40) and augite (Wo 42) may sometimes be found (samples 7 and 8).

Porphyritic dikes (3, 4, 6 of Table 1 a) are represented by latibasalts. The pheno- and microphenocrysts are pink augite (Wo 44–35), plagioclase (An 60–40), Ti–magnetite and weathered olivine. The groundmass is made up of augite, plagioclase, Ti–magnetite, alkali–feldspar and biotite. Cr–spinel phenocrysts occur only in sample 4, in which biotite becomes abundant and olivine phenocrysts are very large.

Nomenclature and petrochemistry

The dikes were classified on a chemical basis[1] (Tables 1 a and 1 b), taking into account both petrographic and mineralogical data (see later).

The nomenclature adopted is based on the classificative diagram of De La Roche et al. (1980), modified by Bellieni et al. (1981). Fig. 2 shows that the

[1] Major and trace elements were determined by X-ray fluorescence (Leoni & Saitta, 1976, and references therein); ferrous iron was determined by means of redox titration; L.O.I. was determined by heating at 1100 °C for 12 hours and corrected assuming all ferrous iron as oxidated. Mineral chemistry was performed on an automated ARL electronic microprobe.

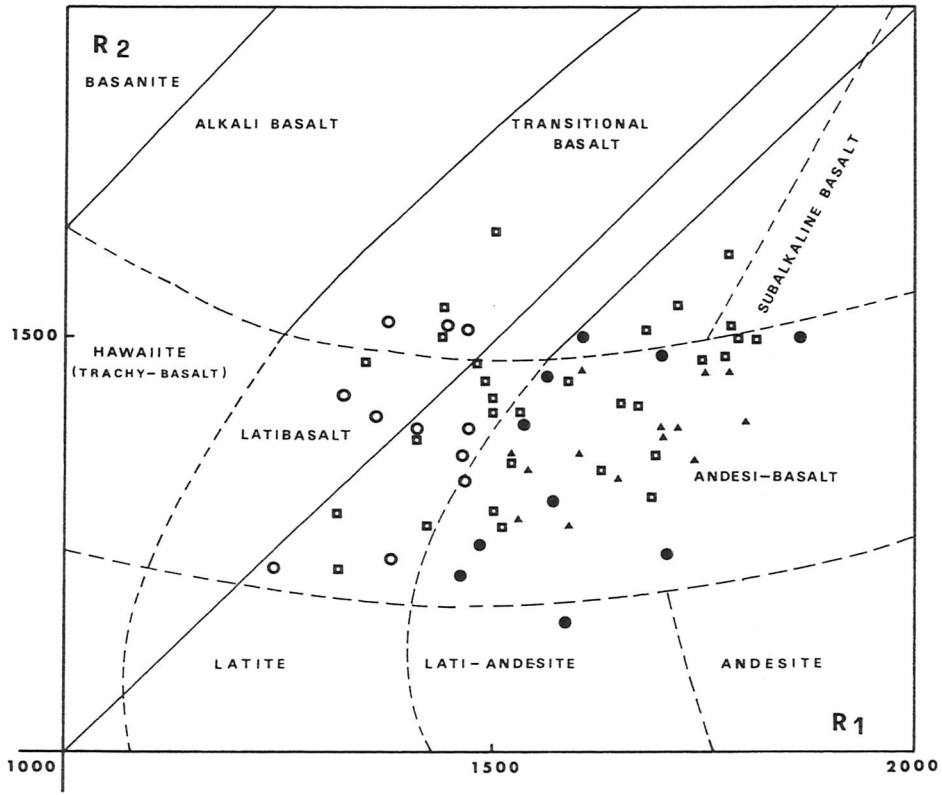

Fig. 2. Distribution of volcanics in the classificative diagram of De La Roche et al. (1980, dashed lines), modified after Bellieni et al. (1981) for alkaline, transitional and subalkaline basalt fields (solid lines). $R_2 = 6\ Ca + 2\ Mg + Al$; $R_1 = 4\ Si - 11\ (Na + K) - 2(Fe + Ti)$.
Open circles: latibasalt suite; *dots:* andesi-basalt suite; *triangles:* high-Ti andesi-basalts from Guata-Bom Jardin and Racinha-Encruzilhada das Anta (RA and GB series respectively; Bellieni et al., 1982); *squares:* high-Ti sills from bore-holes in Paranà basin.

dikes fit two main groups: latibasalts and andesi-basalts. A few samples plot in transitional and subalkaline basalt fields, but are to be considered latibasalts (samples 1, 2. 3) and andesi-basalts (sample 11) owing to their low S.I. values, which vary between 25 and 19. It is noteworthy that many andesi-basalts are displaced towards the latibasalt field.

The alkali-silica diagram (Fig. 3) shows that most of the dikes plot in the transitional field of Bellieni et al. (1981) with the exception of samples 4 and 6, which plot in the mildly alkaline field.

The distinction in a group of "alkaline" affinity (latibasalt) and a group of subalkaline affinity (andesi-basalt) made by means of De La Roche et al. (1980)

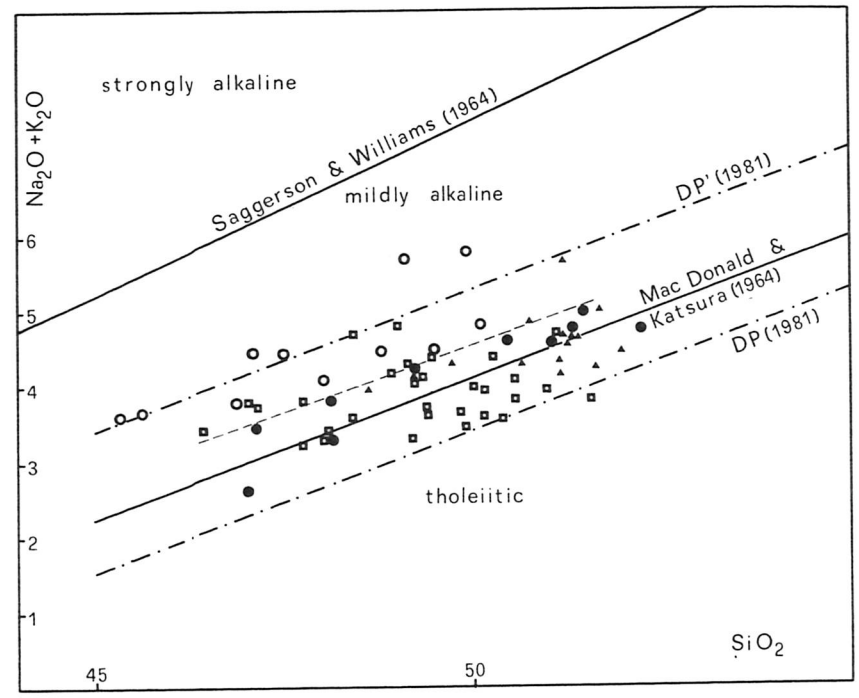

Fig. 3. Alkali-silica diagram. DP and DP′ lines include basaltic rocks of transitional type (Bellieni et al., 1981). Light dashed line divides latibasalt and andesi-basalt suites. Symbols as in Fig. 2.

classification can also be maintained in the alkali-silica diagram: this is graphically shown by a dashed line in Fig. 3.

The distribution of the dikes into these two groups is stressed by the relationships between normative quartz and S.I. (Tables 1 a, 1 b): for a given S.I. value, the subalkaline group always turns out to be higher in normative quartz.

In the A–F–M diagram (Fig. 4), excluding samples 4 and 6 of more alkaline character, the dikes plot between the alkaline and subalkaline curves of Hawaii (MacDonald & Katsura, 1964). They fit better the trends of "transitional" volcanic suites of tholeiitic (Erta Alé; Barberi & Varet, 1970) and alkaline (Boseti; Brotzu et al., 1980) affinities.

Another important chemical character of the dikes studied is their high TiO_2 content (4.2 wt% ± 0.6 as average), that parallels the high concentrations of P_2O_5 (0.81 wt% ± 0.20 as average), Ba (730 pm ± 302) and Sr (735 ppm ± 239).

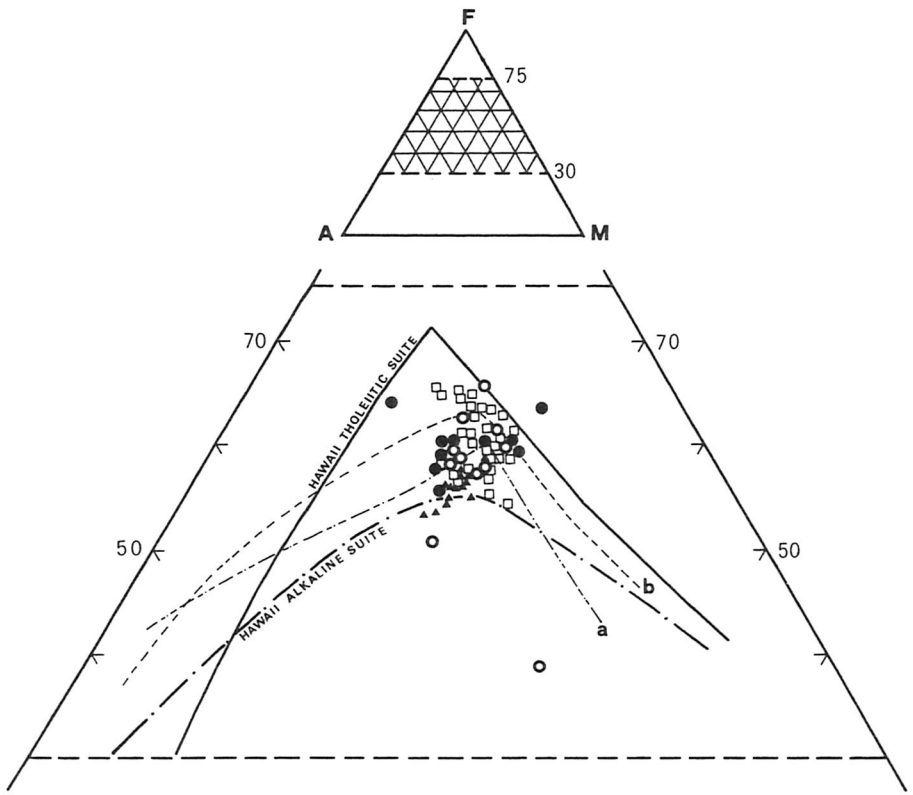

Fig. 4. $A(Na_2O + K_2O)$–$F(FeO_{tot})$–M(MgO) diagram "a": Boseti, Main Ethiopian Rift, transitional alkaline trend (Brotzu et al., 1980); "b": Erta Ale, Afar, transitional tholeiitic suite (Barberi & Varet, 1970). Symbols as in Fig. 2.

Mineral chemistry

Pyroxenes

In both groups the pheno- and microphenocryst pyroxenes are usually represented by augitic and, more rarely, by pigeonitic types (Table 2 and Fig. 5).

The Ca-rich clinopyroxenes of latibasaltic rocks fit the Thingmuli tholeiitic suite (Carmichael, 1964), they have a higher average Ca-content with respect to those of the andesibasaltic ones (Wo 42 and 36 respectively), and plot mainly in the pyroxene field of the Ethiopian transitional basaltic rocks (Brotzu et al., 1981). Moreover, early-crystallized pyroxenes are lower in Ca with respect to the late-crystallized ones, thus showing a distinct alkaline affinity (Brotzu et al., 1981, and references therein). The same behaviour is shown by the Ca-rich pyroxenes with low Wo content of those latibasalts (samples 3 and 10) characterized by pigeonite (sample 10).

The Ca-rich clinopyroxenes of andesi-basalts plot below the Skaergaard trend (Wager & Brown, 1967), and fit the pyroxene field of tholeiites from Hawaii (Fig. 5) and Ethiopia (Brotzu et al., 1981). Unlike the latibasalts, Wo decreases from early- to late-crystallized pyroxenes. This happens even for the clinopyroxene of sample 15, whose Wo content is comparable to that of transitional rock-types with alkaline affinity.

The different behaviour of Ca-rich pyroxenes of lati- and andesi-basalts is stressed if the Di–Hy–Ne normative (CIPW) per cent content of the pyroxenes is considered (Bellieni et al., 1982). Fig. 6 shows that the pyroxenes of latibasalts fit those of transitional rock-types with variable degrees of alkaline affinity, while those of the andesi-basalts clearly belong to melts of substantially tholeiitic character.

Pigeonite occurs only in samples 10 and 21, respectively a latibasalt and an andesi-basalt. The high Wo contents (15.58 and 16.40 % respectively) indicate a metastable character linked to rapid cooling (see Gomes & Ruberti, 1979, and references therein).

Table 1. Major (wt%), trace (ppm) element contents and CIPW norms (Fe_2O_3 = 1.5 %) of latibasalt (section 1 a) and andesi-basalt (section 1 b) suites.

	1	2	3	4	5	6	7	8	9	10	11
	CR38	CR37	CR5	IT4B	CR25	CR33	CR15	CR16	PGC	IT49	CR26
SiO_2	45.32	46.87	45.62	49.08	47.10	49.89	48.78	47.49	50.10	48.03	49.48
TiO_2	5.20	4.61	5.12	4.10	4.34	4.17	4.29	4.21	3.57	4.68	3.31
Al_2O_3	13.44	13.57	13.31	12.49	12.79	14.77	13.23	13.62	12.91	14.11	13.95
Fe_2O_3	4.12	5.92	5.01	2.45	4.51	3.01	5.84	5.52	5.31	3.08	4.46
FeO	9.29	8.61	11.06	6.94	9.07	8.06	7.46	7.51	7.86	10.74	8.75
MnO	0.19	0.20	0.23	0.15	0.19	0.15	0.18	0.17	0.21	0.20	0.19
MgO	5.12	5.03	4.47	8.68	5.02	4.72	4.42	4.22	4.34	4.05	5.04
CaO	9.31	9.32	9.71	7.05	8.45	6.50	8.17	8.55	7.11	8.53	7.47
Na_2O	2.00	2.26	2.06	2.10	2.13	2.72	2.30	2.25	3.23	2.28	2.80
K_2O	1.58	1.51	1.57	3.59	2.30	3.02	2.16	2.14	1.58	1.82	1.67
P_2O_5	0.59	0.76	0.92	0.54	1.16	0.75	1.18	1.17	0.50	0.87	0.72
L.O.I.	2.84	1.34	0.92	2.05	1.95	1.36	1.17	2.42	2.43	0.44	1.19
Total	99.00	100.00	100.00	99.22	99.01	99.12	99.18	99.27	99.15	98.83	99.03
Q	0.46	0.02	-	-	0.81	1.12	3.39	2.20	2.04	2.65	1.20
C	-	-	-	-	-	-	-	-	-	-	-
Or	9.33	8.92	9.27	21.21	13.59	17.84	12.76	12.64	9.33	10.75	9.86
Ab	16.92	19.12	17.43	17.76	18.02	23.01	19.46	19.03	27.33	19.29	23.69
An	23.02	22.42	22.43	14.05	18.54	19.17	19.39	20.74	16.06	22.89	20.56
Di	15.93	15.67	16.53	13.90	13.10	6.71	11.16	11.68	13.29	11.48	9.78
Hy	16.78	19.35	17.07	12.20	19.55	17.89	18.32	17.24	18.13	18.05	22.26
Ol	-	-	1.90	6.70	-	-	-	-	-	-	-
Mt	2.17	2.17	2.17	2.17	2.17	2.17	2.17	2.17	2.17	2.17	2.17
Il	9.87	8.75	9.72	7.78	8.24	7.91	8.14	7.99	6.78	8.88	6.17
Ap	1.39	1.80	2.17	1.27	2.74	1.77	2.79	2.77	1.18	2.06	2.10
Cr	76	60	79	565	20	26	22	20	19	59	105
Ni	79	50	48	115	19	42	17	14	13	47	43
Zr	178	177	183	422	208	411	212	228	89	178	94
Sr	831	690	562	1441	945	878	1074	983	489	563	574
Ba	578	1170	670	1750	1060	840	720	940	529	540	395
Rb	21	29	24	64	61	74	47	41	31	36	34
SI	23.6	22.1	18.9	36.9	22.2	22.2	20.5	20.0	19.9	18.7	22.6

Table 1 a.

	12 CR11	13 CR22	14 CR12	15 CR24	16 CR18	17 CR31	18 TOP	19 CR35	20 CR29	21 IT18
SiO_2	48.12	47.03	47.12	48.09	52.23	49.21	50.44	51.46	51.06	51.33
TiO_2	4.27	4.72	4.34	4.40	3.28	4.93	3.74	3.68	3.25	3.61
Al_2O_3	13.78	13.26	13.32	13.77	14.17	13.74	13.12	13.15	13.37	14.57
Fe_2O_3	4.49	5.67	5.59	5.30	2.90	4.37	5.76	3.43	3.58	2.64
FeO	8.91	9.45	8.27	8.31	8.57	8.83	7.29	9.15	9.75	10.27
MnO	0.19	0.22	0.18	0.20	0.17	0.20	0.21	0.20	0.21	0.19
MgO	5.44	5.38	5.17	4.63	4.11	4.00	3.96	3.99	3.87	2.37
CaO	8.79	9.08	9.21	8.92	7.09	8.66	7.45	7.07	7.90	7.04
Na_2O	2.18	1.13	2.09	2.20	2.20	2.27	2.95	3.04	2.65	2.38
K_2O	1.11	1.49	1.35	1.65	2.55	1.96	1.66	1.95	1.91	2.35
P_2O_5	0.77	0.81	0.63	0.79	0.64	0.63	0.83	0.91	0.89	0.90
L.O.I.	0.98	1.77	1.82	0.83	1.15	0.25	1.79	0.97	0.56	1.22
Total	99.03	100.01	99.09	99.09	99.06	99.05	99.20	99.00	99.00	98.87
Q	3.36	5.26	1.82	2.59	6.92	4.06	4.29	4.57	4.37	7.57
C	-	-	-	-	-	-	-	-	-	-
Or	6.55	8.80	7.97	9.75	15.06	11.58	9.81	11.52	11.28	13.88
Ab	18.44	9.56	17.68	18.61	18.61	19.20	24.96	25.72	22.42	20.13
An	24.53	26.70	22.97	22.82	21.25	21.51	17.65	16.47	18.94	22.13
Di	11.60	10.83	15.41	13.52	8.07	14.42	11.59	10.56	12.11	5.87
Hy	21.15	23.60	19.07	18.19	17.91	14.70	17.43	17.70	18.65	16.79
Ol	-	-	-	-	-	-	-	-	-	-
Mt	2.17	2.17	2.17	2.17	2.17	2.17	2.17	2.17	2.17	2.17
Il	8.10	8.96	8.24	8.35	6.22	9.36	7.10	6.98	6.17	6.85
Ap	1.82	1.91	1.49	1.87	1.51	1.49	1.96	2.15	2.10	2.13
Cr	48	34	47	61	25	6	19	19	40	2
Ni	58	46	56	56	40	66	15	11	32	24
Zr	178	200	180	179	202	247	225	232	200	217
Sr	636	840	646	666	478	861	585	619	506	486
Ba	600	630	488	597	520	803	662	605	563	660
Rb	31	34	27	37	91	40	40	44	41	47
SI	25.1	23.9	23.6	21.5	20.5	19.1	18.8	18.8	18.1	12.0

Table 1 b.

Olivine

The only analysable olivine crystal (Table 3) belonging to andesi-basalt 20 has a high fayalite content, ranging from 72.9 to 74.4 %.

It is also noteworthy that Ca-rich pyroxenes coexisting with olivine (or pigeonite) have the lowest Wo contents (up to 32.6 %). They plot in the pyroxene quadrilateral (Fig. 5) roughly at the Fe-closure of the two-pyroxene field (Roeder & Osborn, 1966).

The Fe/Mg ratio of olivine (and pigeonite) relative to those of coexisting Ca-rich clinopyroxenes are somewhat higher, for example, than those concerning the compositional trends of Skaergaard intrusion (Wagner & Brown, 1967), probably as a consequence of higher Fe/Mg ratios in the melts at the moment of crystallization.

Plagioclase

Plagioclase crystals are always zoned and show a compositional range from labradorite to andesinic oligoclase (Table 4). No relevant differences were

Table 2. Averaged microprobe analyses of selected clinopyroxenes of latibasalt (2 a) and andesi-basalt (2 b) suites. E: early crystallization; L: late crystallization; P: pigeonite.

	1E CR38	1L CR38	2E CR37	2L CR37	3E CR5	3L CR5	4E IT4B	4L IT4B	6E CR33	6L CR33	8E CR16	8L CR16
SiO_2	48.00	45.69	49.98	48.99	51.50	49.75	51.03	50.28	50.86	48.37	48.64	47.58
TiO_2	2.87	3.08	1.73	2.12	0.99	1.43	1.92	1.90	1.62	2.57	2.60	2.48
Al_2O_3	4.95	6.41	4.13	4.43	2.31	3.68	2.90	3.41	3.11	4.52	5.06	5.54
FeO_t	9.02	11.66	11.40	11.02	11.80	12.30	8.31	8.25	9.46	10.79	10.63	11.68
MnO	0.21	0.19	0.24	0.20	0.25	0.23	0.18	0.17	0.23	0.25	0.19	0.17
MgO	14.36	12.06	13.67	13.02	16.49	14.61	15.61	14.77	14.69	13.81	13.32	12.41
CaO	19.95	20.40	18.56	19.85	16.28	16.82	18.91	20.97	20.29	19.46	19.25	19.40
Na_2O	0.42	0.47	0.38	0.43	0.10	0.10	0.53	0.54	0.39	0.45	0.47	0.54
Cr_2O_3	0.08	0.11	-	-	0.15	0.14	0.32	0.13	-	-	-	-
Total	99.86	100.07	100.09	100.06	99.87	99.06	99.71	100.42	100.62	100.22	100.16	99.80
Fe_2O_3*	2.62	4.73	8.25	1.52	0.32	-	0.28	2.54	1.52	2.81	1.00	2.45
Si	1.788	1.719	1.870	1.837	1.918	1.881	1.893	1.855	1.880	1.805	1.818	1.792
Al^{IV}	0.212	0.281	0.130	0.163	0.082	0.119	0.107	0.145	0.120	0.195	0.182	0.208
Σ	2.000	2.000	2.000	2.000	2.000	2.000	2.000	2.000	2.000	2.000	2.000	2.000
Al^{VI}	0.006	0.004	0.053	0.032	0.020	0.045	0.020	0.004	0.016	0.004	0.041	0.038
Fe^{2+}	0.208	0.233	0.350	0.303	0.359	0.389	0.250	0.184	0.250	0.258	0.304	0.298
Fe^{3+}	0.073	0.134	0.007	0.043	0.009	-	0.008	0.071	0.042	0.079	0.028	0.069
Mg	0.797	0.676	0.762	0.727	0.915	0.823	0.863	0.812	0.809	0.768	0.742	0.696
Mn	0.007	0.006	0.008	0.006	0.008	0.007	0.006	0.005	0.007	0.008	0.006	0.005
Ti	0.080	0.087	0.049	0.060	0.028	0.041	0.054	0.053	0.045	0.072	0.073	0.070
Cr	0.002	0.003	-	-	0.004	0.004	0.009	0.004	-	-	-	-
Ca	0.796	0.822	0.744	0.797	0.650	0.681	0.752	0.829	0.802	0.778	0.771	0.783
Na	0.030	0.034	0.028	0.031	0.007	0.007	0.036	0.039	0.028	0.033	0.034	0.039
Σ	2.000	2.000	2.000	2.000	2.000	1.998	2.000	2.000	2.000	2.000	2.000	2.000
Ca	42.32	43.93	39.76	42.48	33.49	35.98	40.02	43.61	41.99	41.14	41.65	42.30
Mg	42.37	36.13	40.73	38.75	47.14	43.48	45.93	42.71	42.36	40.61	40.09	37.60
Fe**	15.31	19.94	19.51	18.76	19.37	20.54	14.05	13.68	15.65	18.24	18.26	20.10

* Fe_2O_3, according to Papike et al. (1974); ** including Fe^{3+} and Mn.

Table 2 a.

observed for the plagioclase of lati- and andesi-basalts, allowance being made for a wider compositional range (An 63–30) and more pronounced zoning of plagioclases of andesi-basalts. The plagioclase xenocrysts (samples 7 and 8) are andesinic (An 40–45) and are sometimes jacketed by alkali feldspars.

Fe–Ti oxides and Cr-bearing spinels

Fe–Ti phases are represented mainly by high-Ti magnetite and ilmenite (Table 5). Equilibration temperatures and log fO_2, calculated on coexisting Ti– magnetite and ilmenite pairs (Buddington & Lindsley, 1964) range from 900 to 1120 °C and from –12.8 to –9.30 respectively (Fig. 7). The fO_2 and temperature values define a distribution pattern lying between the QFM and NNO buffer curves.

The above-mentioned temperatures substantially reveal post-eruptive re-equilibration. Only for latibasalt 4 can the temperature of 1120 °C probably represent that of quenching.

In sample 4 phenocrysts of strongly zoned Cr–spinel (Cr_2O_3; core = 50.5 %,

	15E CR24	15L CR24	16E CR18	16L CR18	17E CR31	17L CR31	20E CR29	20L CR29	21E IT18	21L IT18	21P IT18
SiO_2	47.90	49.00	50.74	50.69	50.05	50.15	51.00	50.60	51.41	50.56	50.70
TiO_2	2.27	1.79	1.31	1.15	1.51	1.37	0.83	0.65	1.11	1.03	0.62
Al_2O_3	4.80	3.79	2.80	2.29	3.59	2.98	1.63	1.45	2.05	2.10	0.76
FeO_t	12.08	13.58	10.93	11.70	10.81	11.95	16.37	18.50	14.49	15.52	29.65
MnO	0.26	0.36	0.37	0.42	0.22	0.22	0.36	0.39	0.35	0.33	0.57
MgO	12.37	12.67	15.81	15.18	15.81	15.89	13.10	12.25	15.33	13.25	10.84
CaO	19.66	18.31	17.86	17.82	16.93	16.13	16.44	15.21	15.50	16.39	7.50
Na_2O	0.55	0.48	0.37	0.40	0.47	0.46	0.10	0.10	0.30	0.30	0.09
Cr_2O_3	-	-	-	-	0.26	0.06	0.02	0.02	-	-	-
Total	99.89	99.98	100.19	99.65	99.65	99.21	99.85	99.17	100.54	99.48	100.13
Fe_2O_3*	3.12	2.23	2.48	2.32	2.08	2.32	-	-	1.05	0.53	-
Si	1.805	1.851	1.881	1.898	1.863	1.879	1.944	1.956	1.920	1.927	1.975
Al^{IV}	0.195	0.149	0.119	0.101	0.137	0.121	0.056	0.044	0.080	0.073	0.025
Σ	2.000	2.000	2.000	1.999	2.000	2.000	2.000	2.000	2.000	2.000	2.000
Al^{VI}	0.018	0.019	0.003	-	0.020	0.010	0.018	0.022	0.010	0.021	0.010
Fe^{2+}	0.292	0.366	0.270	0.301	0.278	0.309	0.522	0.598	0.423	0.480	0.979
Fe^{3+}	0.089	0.063	0.069	0.065	0.058	0.066	-	-	0.029	0.015	-
Mg	0.695	0.713	0.874	0.847	0.877	0.887	0.744	0.706	0.853	0.753	0.638
Mn	0.008	0.012	0.012	0.013	0.007	0.007	0.012	0.013	0.011	0.011	0.019
Ti	0.064	0.051	0.037	0.032	0.042	0.039	0.024	0.019	0.031	0.030	0.018
Cr	-	-	-	-	0.008	0.002	0.001	0.001	-	-	-
Ca	0.794	0.741	0.709	0.715	0.675	0.647	0.672	0.630	0.620	0.669	0.317
Na	0.040	0.035	0.027	0.029	0.034	0.033	0.007	0.007	0.022	0.022	0.015
Σ	2.000	2.000	2.000	2.002	2.000	2.000	1.999	1.996	2.000	2.000	1.997
Ca	42.28	39.10	36.66	36.84	35.62	33.77	34.64	32.56	32.02	34.70	16.40
Mg	37.01	37.63	45.19	43.64	46.28	46.29	38.40	36.48	44.06	39.06	32.98
Fe**	20.71	23.27	18.15	19.53	18.10	19.94	26.96	30.93	23.92	26.24	50.62

Table 2 b.

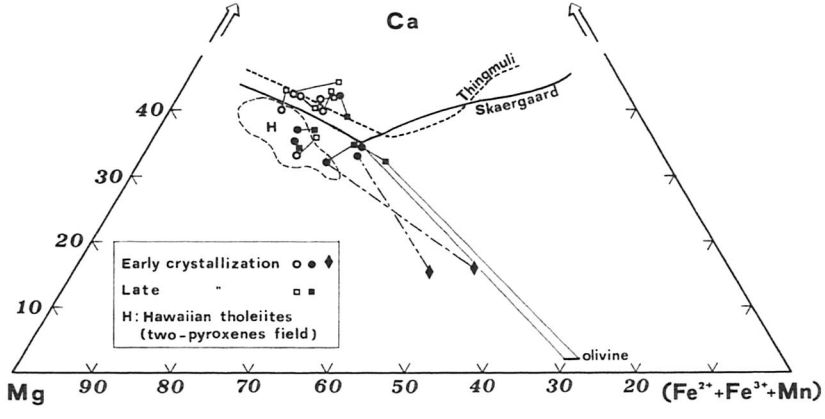

Fig. 5. Pyroxene quadrilateral showing plot of clinopyroxene and olivine of lati- and andesi-basalt suites. Symbols as in Fig. 2.

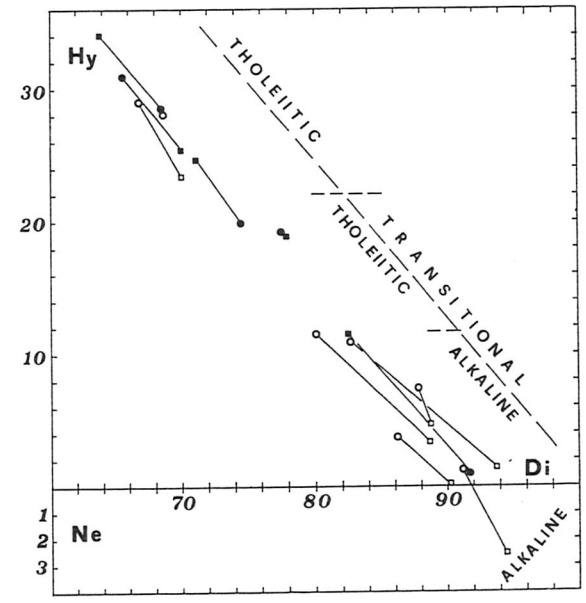

Fig. 6. Normative (CIPW) Di vs Hy–Ne for Ca-rich pyroxenes. Symbols as in Fig. 2.

Table 3. Averaged microprobe analyses of olivine (C: core; R: rim) (sample 20).

	20E CR29	20L CR29
SiO_2	31.68	31.97
TiO_2	0.07	0.08
FeO	54.92	55.87
MnO	0.77	0.67
MgO	11.51	10.62
CaO	0.21	0.16
Total	99.16	99.57
Si	0.995	1.002
Ti	0.002	0.002
Fe^{2+}	1.442	1.464
Mn	0.021	0.018
Mg	0.539	0.505
Ca	0.007	0.005
Σ	3.006	2.996
Fo	27.1	25.6
Fa	72.9	74.4

rim = 14.8 wt%, Table 5) associated with olivine, can be found. The increase of ulvospinel–magnetite solid solution towards the crystal rim is very similar to that occurring in the mafic lavas of Queenland (Australia) and Makaopuhi Lake (Hawaii). This compositional variation is attributed by Evans & Moore

Table 4. Representative microprobe plagioclase compositions.

	3E CR5	3L CR5	6E CR33	6L CR33	8E CR16	8L CR16	15E CR24	15L CR24	16E CR18	16L CR18	17E CR31	17L CR31	21E IT18	21L IT18
SiO_2	54.25	56.65	55.33	57.85	57.25	58.20	57.12	60.63	52.20	57.27	53.97	57.02	55.06	61.23
Al_2O_3	28.51	27.37	28.52	27.02	27.17	26.23	27.54	24.42	30.10	27.11	29.56	27.22	28.40	24.59
CaO	10.86	9.36	10.62	8.79	9.06	8.06	9.39	6.00	12.65	9.00	11.79	9.15	10.58	6.00
Na_2O	5.03	5.93	5.08	6.11	5.94	6.44	5.98	7.65	4.03	6.21	4.60	5.90	5.18	7.55
K_2O	0.46	0.56	0.80	0.92	0.87	0.92	0.59	0.87	0.44	0.50	0.52	0.81	0.60	1.16
Total	99.11	99.86	100.35	100.68	100.29	99.85	100.62	99.57	99.41	100.09	100.44	100.10	99.81	100.55
Or	2.7	3.3	4.7	5.4	5.1	5.4	3.5	5.2	2.6	2.9	3.1	4.8	3.5	6.9
Ab	42.9	50.2	42.8	51.3	50.1	54.5	50.2	64.9	34.3	52.5	38.7	49.8	43.9	63.5
An	54.4	46.5	52.5	43.3	44.8	40.1	46.3	29.9	63.1	44.6	58.2	45.4	52.6	29.6

(1968) and EWART et al. (1980) to post-eruption solid state alteration of original chromites during cooling.

Discussion

The petrographic, mineralogical and geochemical data show that the dikes studied have a transitional character with more or less pronounced alkaline or tholeiitic affinity.

The variation diagrams on major and trace elements (Figs. 8 and 9) reveal that the distribution pattern does not show any simple or well-defined trends, and that the solidification index (S.I.) mainly ranges from 24 to 18, excluding the "anomalous" sample 4 (S.I. = 36.9) and the most evolved one (21; S.I. = 12.0).

A notable feature is that, for the same S.I. value, the dikes show important variations of many element concentrations, even within the same rock-types. Instead, more defined trends appear to exist when the relationships between the trace elements are considered. Fig. 10, for example, shows a general increase of Rb and Ba and a decrease in Ni and Cr, parallel to the increase in Zr.

Similar geochemical features (Figs. 8–10) are also shown by the high-Ti basaltic flows of Serra Geral (Santa Catarina and Rio Grande do Sul, BELLIENI et al., 1982) and by 27 bore-hole sills (COMIN-CHIARAMONTI, MELFI & PICCIRILLO, unpublished data) of the northern Paranà basin. However, it is important to note that these high-Ti flows and sills (Ti-PB) reveal many differences with respect to the dikes studied (Ti-CD).

The alkali-silica diagram (Fig. 3) shows that the Ti-PB plot in the transitional field and that many samples have more pronounced tholeiitic affinity than that of Ti-CD. This fact is also apparent in Fig. 2, where only part of the bore-hole sills straddle the andesi-basalt/latibasalt boundary.

From the geochemical viewpoint the Ti-PB are characterized with respect to Ti-CD by lower average concentrations of TiO_2 (3.3 ± 0.3 %), P_2O_5 (0.55 ± 0.14 %), Ba (618 ± 135 ppm) and Sr (537 ± 130 ppm). Moreover, the Zr

Table 5: Averaged microprobe analyses of selected coexisting opaques occurring in latibasalt and andesi-basalt suites. Fe_2O_3 and FeO were calculated on ulvospinel basis and ilmenite basis for spinel and rhombohedral phases respectively, according to CARMICHAEL (1967).

Magnetites	2 CR37	4 IT4B	6 CR33	16 CR18	17 CR31	20 CR29	21 IT18
SiO_2	0.40	0.27	0.16	0.60	0.15	0.13	0.10
TiO_2	19.78	24.64	20.70	17.93	18.40	17.52	22.02
Al_2O_3	1.05	1.91	1.40	3.21	0.95	1.04	1.04
Cr_2O_3	0.13	0.80	0.36	1.57	0.16	0.14	0.32
FeO	73.56	68.55	73.76	72.71	76.70	75.98	72.80
MnO	0.69	0.25	0.27	0.10	0.21	0.37	0.40
MgO	0.63	0.23	0.21	0.44	0.16	0.11	0.04
CaO	0.44	0.08	0.05	0.04	0.03	0.02	0.02
Total	96.68	96.76	96.91	96.60	96.76	95.31	96.74
Ulvospinel basis							
FeO	47.83	53.49	49.98	48.09	48.02	46.70	51.11
Fe_2O_3	28.58	16.73	26.42	27.35	31.86	32.50	24.10
Σ	99.53	98.43	99.55	99.33	99.94	98.50	99.15
Ulv(%)	57.71	72.16	59.78	54.07	53.02	51.22	63.55
Ilmenite basis							
FeO	35.64	38.49	37.43	36.85	36.86	36.08	37.81
Fe_2O_3	42.13	33.40	40.36	39.84	44.26	44.33	38.87
Σ	100.89	100.10	100.94	100.58	101.18	99.74	100.62
Ilmenites							
SiO_2	0.19	0.08	0.04	0.13	0.01	0.06	0.03
TiO_2	45.51	45.96	49.69	48.45	45.90	46.64	47.19
Al_2O_3	0.10	0.26	0.23	0.07	0.43	0.08	0.18
Cr_2O_3	0.06	0.04	0.30	0.10	0.30	0.06	0.21
FeO	50.88	51.62	46.93	48.20	49.50	50.64	49.16
MnO	0.71	0.49	0.31	0.42	0.29	0.70	0.47
MgO	0.68	0.05	0.94	0.51	2.20	0.36	0.89
CaO	0.18	0.05	0.06	0.07	0.03	0.01	0.07
Total	98.31	98.55	98.50	97.94	98.66	98.55	98.20
FeO	39.01	40.81	42.69	42.33	37.03	40.68	40.34
Fe_2O_3	13.19	12.01	4.72	6.53	13.86	11.07	9.80
Σ	99.63	99.75	98.98	98.60	100.05	99.66	99.18
R_2O_3	12.79	11.91	5.16	6.49	13.98	10.76	9.86
T(°C)	1062	1120	916	898	1050	968	1044
-log fO_2	9.65	9.30	12.60	12.75	9.75	11.05	10.25

Cromites	4E IT4B	4L IT4B
SiO_2	0.10	0.10
TiO_2	2.88	6.18
Al_2O_3	6.64	4.74
Cr_2O_3	50.50	14.81
Fe_2O_3	10.94	42.22
FeO	23.23	31.42
MnO	0.52	0.40
MgO	6.68	0.06
CaO	-	0.07
Total	101.49	100.00
Si	0.027	0.029
Ti	0.587	1.354
Al	2.115	1.629
Cr	10.797	3.415
Fe^{3+}	2.222	9.249
Fe^{2+}	5.242	7.648
Mn	0.119	0.099
Mg	2.713	0.026
Ca	0.000	0.022
O	32.000	32.000

vs. Ni and Cr diagrams (Fig. 10) clarify the possibility of Ti-CD primary melts with lower Zr concentration with respect to those of the corresponding Ti-PB ones, if the relative distribution patterns are interpreted as liquid lines of descent related to crystal fractionation processes (see also BELLIENI et al., 1982).

While in the AFM diagram (Fig. 4) only part of the bore-hole sills reveal

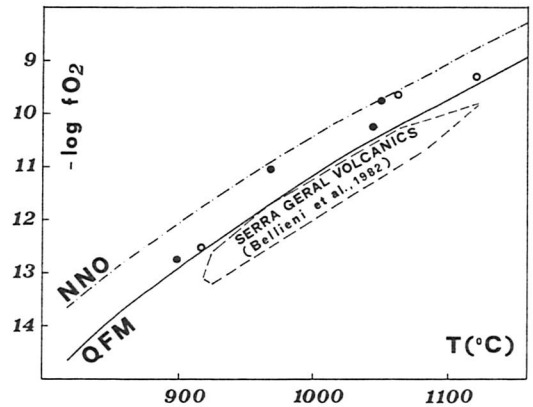

Fig. 7. Relationships between ilmenite–magnetite pairs, plotted in log fO_2 vs T(OC) diagram, with QFM-NNO buffer curves (after Powell & Powell, 1977, and references therein).

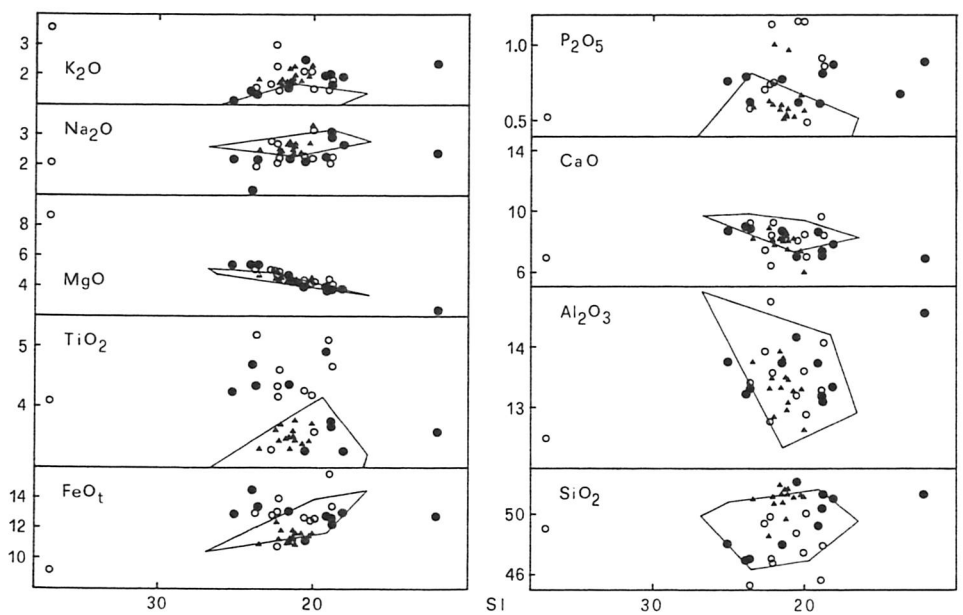

Fig. 8. Variation diagrams of S.I. [Solidification Index: 100 $Mg/MgO + FeO_t + Na_2O + K_2O$)] vs major elements (wt%). Contoured fields represent bore-hole sills. Symbols as in Fig. 2.

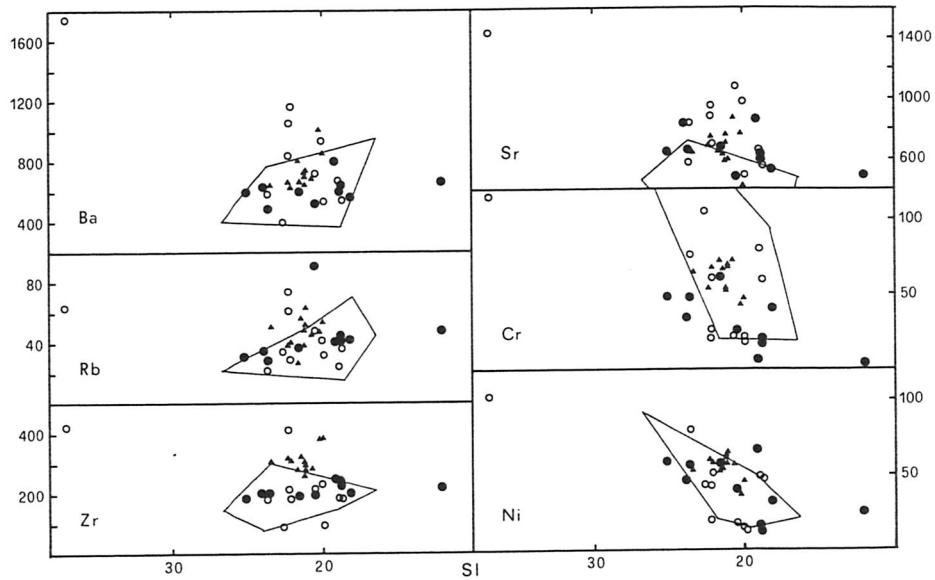

Fig. 9. Variations diagrams of S.I. vs trace elements (ppm). Symbols as in Fig. 2.

higher Fe-enrichment than other high-Ti rocks, important differences between Ti-PB and Ti-CD concern fO_2. The T(°C) vs log fO_2 diagram (Fig. 7) in effect shows that the Ti-CD define a curve between the QFM and NNO buffers, while the Ti-PB are characterized by a lower fO_2 (below the QFM buffer, Bellieni et al., 1982).

Concluding remarks

Comparative analysis of the high-Ti basaltic rocks of Southern Brazil reveals that, proceeding from west to east, melt compositions change from tholeiitic to transitional with alkaline affinity. If related to a lower partial melting degree for Ti-CD, this fact may explain their higher concentrations in Ti, P and other incompatible elements (e.g. Ba, Rb) with respect to the Ti-PB. However, it is important to stress that in this case the somewhat large variability of incompatible element contents within the same rock-types (cf. Tables 1 a, 1 b) implies mantle "heterogeneity", as also suggested by the close association of low- and high-Ti tholeiitic andesi-basalts in the Serra Geral formation (Bellieni et al., 1982, and unpublished data). In any case, this problem requires further extensive data to be examined in detail.

If the available radiometric ages (124–138 m.y., Lower Cretaceous) on only a few dikes are assumed as representative of all the dike activity studied, it fol-

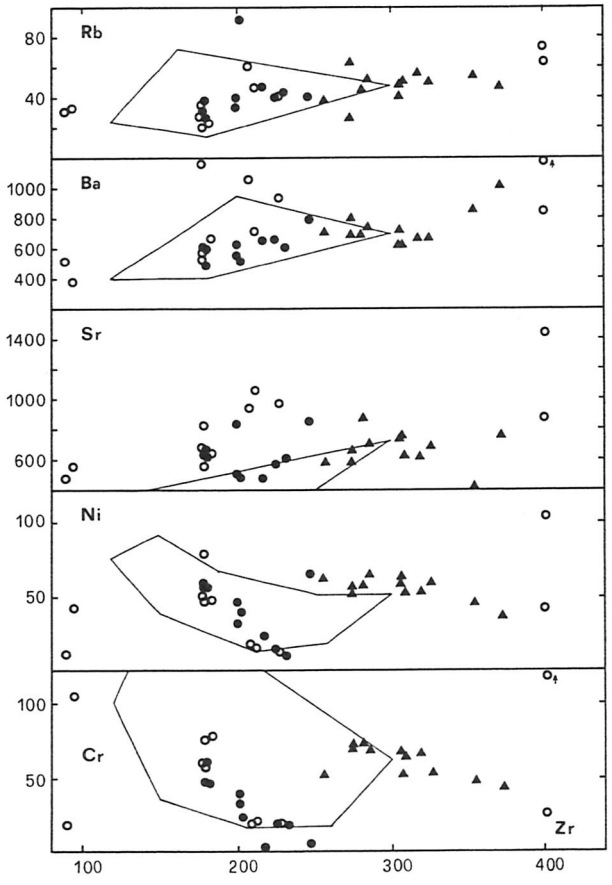

Fig. 10. Zr vs trace elements (ppm). Symbols as in Fig. 2.

lows that there was a "contemporaneous" outpouring of tholeiitic and transitional basaltic magmas in both the western and eastern parts of the Paranà basin.

In this picture the eastern Paranà basin may have represented, at that time, a peripheral zone (lower melting degree) with respect to the area(s) of higher thermal anomaly (higher melting degree). On the other hand, it is noteworthy that during the Upper Cretaceous a very pronounced alkaline magmatism developed essentially in the outer eastern regions of the Paranà basin (Ulbrich & Gomes, 1981).

Acknowledgements

This work was financed by the Italian Minsistry of Public Education and the C.N.R. (National Council for Research).

Thanks are due to Prof. S. Sinigoi for microprobe analyses. The C.N.R. is acknowledged for maintenance of an ARL microprobe at the "Istituto di Mineralogia e Petrografia" of the University of Modena (Italy).

References

Amaral, G., Cordani, U. G., Kawashita, U. & Reynolds, J. H. (1966): Potassium-argon dates of basaltic rocks from southern Brazil. – Geoch. Cosm. Acta, **30:** 159–189.

Barberi, F. & Varet, J. (1970): The Erta Ale range (Danakil Depression, northern Afar, Ethiopia). – Bull. volc., **34:** 848–917.

Bellieni, G., Brotzu, P., Comin-Chiaramonti, P., Ernesto, M., Melfi, A. J., Pacca, I. G., Piccirillo, E. M. & Stolfa, D. (1982): Petrological and palaeomagnetic data on the stratoid basalt to rhyolite sequences of Southern Paranà plateau (Brazil). – An. Acad. brasil. Ciênc. (in press).

Bellieni, G., Piccirillo, E. M. & Zanettin, B. (1981): Classification and nomenclature of basalts. IUGS, Subcommission on Systematics of Igneous Rocks. – Circ., **34:** Contr. 87, Cambridge.

Brotzu, P., Morbidelli, L., Piccirillo, E. M. & Traversa, G. (1980): Volcanological and magmatological evidence of the Boseti volcanic complex (main Ethiopian rift). – In: Geodynamic Evolution of the Afro-Arabian Rift System. Acc. Naz. Lincei, Roma, **47:** 317–366.

Brotzu, P., Ganzerli-Valentini, M. T., Morbidelli, L., Piccirillo, E. M., Stella, R. & Traversa, G. (1981): Basaltic volcanism in the northern sector of the main Ethiopian rift. – Jour. of Volc. and Geoth. Res., **10:** 365–382.

Buddington, A. F. & Lindsley, D. H. (1964): Iron–Titanium oxide minerals and synthetic equivalents. – Journ. Petrol., **5:** 310–357.

Carmichael, I. S. E. (1964): The petrology of Thingmuli, a Tertiary Volcano in Eastern Iceland. – Journ. Petrol., **5:** 435–460.

– (1967): The Iron–Titanium oxide of salic volcanic rocks and their associated ferromagnesian silicates. – Contr. Mineral. Petrol., **14:** 36–64.

Damasceno, E. C. (1966): Estudo preliminar dos diques de rochas basicas e ultrabasicas da região de Ubatuba, Estado de São Paulo. – An. Acad. bras. Ciênc., **38:** 293–304.

Evans, B. W. & Moore, G. (1968): Mineralogy as a function of depth in prehistoric Macaopuhi tholeiitic lava lake, Hawaii. – Contr. Mineral. Petrol., **17:** 85–115.

Ewart, A., Baxter, K. & Ross, J. A. (1980): The petrology and petrogenesis of the Tertiary anorogenic mafic lavas of southern and central Queensland, Australia. Possible implication for crustal thickening. – Contr. Mineral. Petrol., **75:** 129–152.

Gomes, C. B. (1974): Mineralogia do dique de Toninhas, Ubatuba, litoral Norte do Estado de São Paulo: Feldspatos. – Rev. Bras. Geoc., **4:** 80–87.

Gomes, C. B. & Ruberti, E. (1979): Mineralogia do dique de Toninhas, Ubatuba, litoral Norte do Estado de São Paulo: Piroxênios. – Boletim Mineralogico, Recife, **6: 55–66.**

Gomes, C. B. & Berenholc, M. (1980): Some geochemical features of the Toninhas dike, Ubatuba, State of São Paulo, Brazil. – An. Acad. brasil. Ciênc., **52:** 339–346.

La Roche, de, H., Le Terrier, P., Grandclaude, P. & Marchal, M. (1980): A classification of volcanic and plutonic rocks using R_1R_2-diagram and major-element analyses. Its relationships with current nomenclature. – Chem. Geol., **29:** 183–210.

Leoni, L. & Saitta, M. (1976): X-ray fluorescence analysis of 29 trace elements in rock and mineral standards. – Rend, SIMP, **32:** 497–510.

MacDonald, G. A. & Katsura, T. (1964): Chemical composition of Hawaiian lavas. – Journ. Petrol., **5:** 82–133.

Melfi, A. J. (1967): Potassium-Argon dates for core samples of basaltic rocks from Southern Brazil. – Geoch. Cosm. Acta, **31:** 1079–1089.

Minioli, B., Ponçano, W. L. & De Oliveira, S. M. B. (1971): Extensão geografica do vulcanismo basaltico do Brasil meridional. – An. Acad. brasil. Ciênc., **43:** 433–437.

Papike, J. J., Cameron, K. & Baldwin, K. (1974): Amphiboles and pyroxenes: characterization of other than quadrilateral components and estimates of ferric iron from microprobe data. – Geol. Soc. Am., abstract with programs, **6:** 1053–1054.

Powell, R. & Powell, M. (1977): Geothermometry and oxygen barometry using coexisting iron–titanium oxides. A reappraisal. – Mineral. Mag., **41:** 257–263.

Roeder, P. L. & Osborn, E. F. (1966): Experimental data for the system MgO–FeO–Fe_2O_3–$CaAl_2Si_2O_8$–SiO_2 and their petrogenetic implications. – Am. Journ. Sci., **264:** 428–480.

Saggerson, E., P. & Williams, L. A. J. (1964): Ngurumanite from southern Kenia and its bearing on the origin of rocks in the northern Tanganika alkaline district. – Journ. Petrol., **5:** 40–81.

Siedner, G. & Mitchell, J. G. (1976): Episodic mesozoic volcanism in Namibia and Brazil: A K–AR isochron study bearing on the opening of the south Atlantic. – Earth Planet. Sci. Letters, **30:** 292–302.

Wager, L. R. & Brown, G. M. (1968): Layered Igneous rocks. – Edinburgh: Oliver and Boyd, Ltd., 588 p.

Ulbrich, H. H. G. J. & Gomes, C. B. (1981): Alkaline rocks from continental Brazil. – Earth Sci. Rev., **17:** 135–154.

Manuscript received by the editor November 10, 1982.

Authors' addresses:

Piero Comin-Chiaramonti and Enzo Michele Piccirillo, Istituto di Mineralogia e Petrografia dell'Università, Piazzale Europa 1, I-34100 Trieste, Italy.

Celso De Barro Gomes, Instituto de Geociências, Universidade de São Paulo, CEP 0100, São Paulo, Brazil.

Giorgio Rivalenti, Istituto di Mineralogia dell'Università, Corso Ercole I d'Este, 44100, Ferrara, Italy.